FISEVIER

Contents lists available at ScienceDirect

# Computational Materials Science

journal homepage: www.elsevier.com/locate/commatsci





# 2D Ni<sub>0.25</sub>Mn<sub>0.75</sub>O<sub>2</sub>: A high-performance cathode for multivalent ion batteries

Diana Liepinya <sup>a,b</sup>, Robert Shepard <sup>a,c</sup>, Manuel Smeu <sup>a,\*</sup>

- a Department of Physics, Binghamton University, Binghamton, NY, United States of America
- <sup>b</sup> University of Maryland, College Park, MD, United States of America
- <sup>c</sup> Department of Science and Mathematics, Alvernia University, Reading, PA, United States of America

#### ARTICLE INFO

# Keywords: Density functional theory 2D Nickel manganese oxide Mono-/di-/trivalent ions Secondary battery

#### ABSTRACT

Although Li-ion batteries have driven portable energy storage in recent decades, there is increasing concern about their safety, cost, and abundance of constituents. Multivalent ion batteries (MVIBs) have the potential to remedy these issues, but they are limited by the currently known MVIB cathodes, which fail to deliver unanimously favorable voltage, energy density, and diffusion kinetics. We used density functional theory (DFT) to model the performance of Li, Na, Mg, Ca, and Al ions when paired with 2D Ni<sub>0.25</sub>Mn<sub>0.75</sub>O<sub>2</sub>, a novel cathode that uses increased layer separation to improve on the kinetics of its 3D analog. Our calculations yielded maximum voltages of 3.38 V for Na and 2.7 V for Ca, outperforming 2D Na<sub>x</sub>MnO<sub>2</sub> and Na<sub>x</sub>NiO<sub>2</sub>. Diffusion barriers for Li, Na, and Ca are below 300 meV, comparable to existing battery technology and the endpoint 2D cathodes; meanwhile, Mg and Al have prohibitively high diffusion barriers, implying their incompatibility with this cathode. Lastly, density of states calculations and Bader charge analysis show that the cathode becomes conducting following ion adsorption, which is necessary for high-rate performance. 2D Ni<sub>0.25</sub>Mn<sub>0.75</sub>O<sub>2</sub> maintains performance seen with other 2D transition metal oxides while increasing cathode conductivity, indicating that it is a promising candidate for experimental investigation with Li, Na, and Ca ions

## 1. Introduction

Li-ion batteries have outpaced other secondary battery technologies in terms of energy density and cyclability, making them the first choice for portable energy storage in a variety of applications [1]. However, it is believed that Li-ion batteries are reaching a performance ceiling that suggests other innovations are necessary to better meet the quickly growing global demand for energy storage [2]. Certain less-studied alternatives present an opportunity to go beyond what is attainable with current Li-ion technologies, both in regards to energy density and other factors such as safety, cost, and material availability [3].

Contrasting with monovalent lithium, multivalent ion batteries (MVIBs) offer one possible avenue for developing affordable, high-performance batteries. In particular, multivalent (MV) ions such as Ca can carry more charge for a given number of transferred ions [2], making them an especially appealing alternative. The work of Wu et al. has demonstrated this effect in practice by doubling the capacity of  $\alpha$ -MnO<sub>2</sub> by replacing Na<sup>+</sup>, the intercalated ion, with Ca<sup>2+</sup> [4]. However, the relative dearth of research into MV-ion cathodes puts a limiting factor on their development [2], creating a need for further investigation. Recently, MnO<sub>2</sub> has been gaining traction as a MV-ion cathode with high capacities and voltages far exceeding those of

the standard chevrel phase, a popular MVIB cathode [2,5]. However, MnO<sub>2</sub> polymorphs fall short in a variety of ways, including poor kinetics, conversion reactions, and excessive volume change [5,6]. The present study attempts to improve upon kinetics in particular, as it is a common issue in MVIBs [2,7]. There is both experimental [8,9] and computational [10] evidence that 2D MnO<sub>2</sub>, as derived from its layered polymorph, is effective in lowering diffusion barriers. This trend agrees with those found in transition metal oxides (TMOs) [10–12], transition metal disulfides (TMDs) [11], and many other 2D cathode materials [13,14]. An ion adsorbed onto a 2D surface faces fewer physical and electronic obstacles than one intercalated into a 3D material, explaining these trends [13,14]. A study by Xiong et al. [9] also found increased capacity in 2D MnO2 as compared to bulk, suggesting a possibility of increased gravimetric energy density. 2D materials are an untapped resource in their own right, with many possible applications in fields such as energy, electronics, and bioengineering [13,15], increasing the need for understanding of their unique properties.

Although monolayer MnO<sub>2</sub> exhibits improved ionic conductivity, studies by Xiong et al. [9] and Jia et al. [16] reported poor electronic conductivity, describing it as a limiting factor in the rate capability

E-mail address: msmeu@binghamton.edu (M. Smeu).

<sup>\*</sup> Corresponding author.

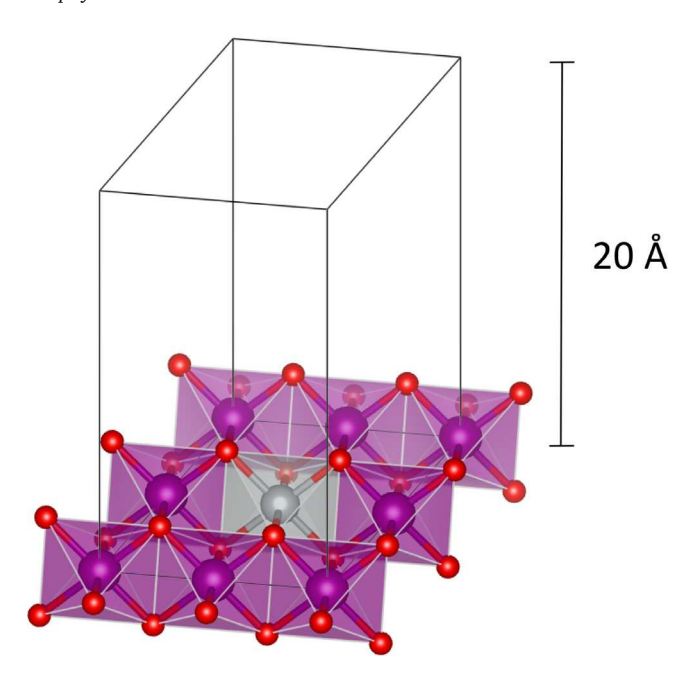


**Fig. 1.** The 2D  $Ni_{0.25}Mn_{0.75}O_2$  unit cell takes the structure of layered  $\delta$ -MnO $_2$  where every fourth Mn is replaced by a Ni atom. Mn (purple) and Ni (gray) atoms reside at centers of octahedra while O (red) are at their vertices. (For interpretation of the references to color in this figure legend, the reader is referred to the web version of this article.)

of their cells. Multiple techniques have been used to improve conductivity in bulk MnO<sub>2</sub>, including integrating conductive materials [16, 17], inducing defects [16], and doping with transition metals [14,15]. The first method, integration of materials like carbon nanotubes and conductive metal oxides, has proved difficult due to high interface energy of MnO<sub>2</sub> and additives [18]. Transition metal doping is more energetically favorable than creating composites; thus, the present paper takes the doping approach. To the best of the authors' knowledge, neither experimental nor computational studies have characterized 2D, transition-metal-doped MnO<sub>2</sub> as a MV-ion cathode. In particular, Ni has been shown to yield significant increases in electronic conductivity in MnO<sub>2</sub> [19,20].

In light of its possible conductivity and diffusion improvements over 3D  $MnO_2$ , the present work used density functional theory (DFT) to study a 2D  $Ni_{0.25}Mn_{0.75}O_2$  cathode vs. a pure metal anode, as represented in Eq. (1):

$$M + \text{Ni}_{0.25}\text{Mn}_{0.75}\text{O}_2 \rightarrow M\text{Ni}_{0.25}\text{Mn}_{0.75}\text{O}_2,$$
 (1)

where M is Li, Na, Mg, Ca, or Al. Fig. 1 shows the 2D Ni $_{0.25}$ Mn $_{0.75}$ O $_2$  unit cell. Despite the overwhelming presence of di- and trivalent Ni in typical electrode materials, tetravalent Ni has also been observed. This system is motivated by recent work by Li et al. who have synthesized layered Na $_{0.5}$ Ni $_{0.25}$ Mn $_{0.75}$ O $_2$  for use as a secondary battery cathode that relies on reversible (Ni $^{2+} \leftrightarrow$  Ni $^{4+}$ ) redox [21]. Further, multiple studies have successfully used spinel Ni $_{0.25}$ Mn $_{0.75}$ O $_2$  as a Li-ion battery cathode, suggesting that although rare, Ni $^{4+}$  can be observed in this context [22,23]. Such bulk TMOs can be chemically or mechanically exfoliated to produce their 2D analogs, providing a possible synthesis method for monolayer Ni $_{0.25}$ Mn $_{0.75}$ O $_2$  [15].

#### 2. Computational methods

Density functional theory [24–26] was used to model the system, as implemented in the Vienna *Ab initio* Simulation Package (VASP) using the projector augmented wave (PAW) method [27]. The Perdew–Burke–Ernzerhof (PBE) exchange–correlation generalized gradient approximation functional was used [28]. All calculations were carried out

with a kinetic energy cutoff for the plane wave basis set of 650 eV and a  $\Gamma$ -centered Monkhorst–Pack k-point grid of  $3 \times 3 \times 1$ , which was sufficient for energy convergence within 1 meV/atom.

To simulate a 2D surface, individual 2 Å-thick layers of NiMn $_3$ O $_8$ , shown in Fig. 1, were separated by 18 Å, resulting in a total cell height of 20 Å. The energies calculated at this distance were within 1 meV to those separated by 27 Å, confirming that interlayer interaction is negligible at those distances. Initially, the structure was fully relaxed with constant volume. The c vector was manually adjusted to remain perpendicular to the a and b vectors. The NiMn $_3$ O $_8$  unit cell was multiplied in both the a and b directions to create a 2 × 2 supercell (Ni $_4$ Mn $_1$ 2O $_3$ 2) with a and b vectors (both 11.04 Å) oriented such that the angle between them was 120°. All further relaxations were performed with these fixed lattice parameters, only allowing ionic motion, in order to maintain interlayer separation. Pure metal anodes underwent full structural relaxations, including lattice vectors. All 3D images were created using the Visualization for Electronic Structural Analysis (VESTA) package [29].

The voltage profile was created according to Eq. (2):

$$V_x = -\left(\frac{E_{M_{x_j} \text{Ni}_4 \text{Mn}_{12} \text{O}_{32}} - E_{M_{x_i} \text{Ni}_4 \text{Mn}_{12} \text{O}_{32}} - (x_j - x_i) E_M}{(x_j - x_i) n}\right), \tag{2}$$

where M is the adsorbed ion,  $E_{M_{x_j} \text{Ni}_4 \text{Mn}_{12} \text{O}_{32}}$  is the energy of the 2D  $\text{Ni}_{0.25} \text{Mn}_{0.75} \text{O}_2$  supercell with an additional adsorbed ion,  $E_{M_{\chi_i} \text{Ni}_4 \text{Mn}_{12} \text{O}_{32}}$  is the energy of the supercell before additional adsorption,  $E_M$  is the energy per atom of the metal anode, and n is the valence of the ion; since all intermediate concentrations are on the convex hull,  $(x_i - x_i) = 1$ . In order to obtain the cathode energies used in Eq. (2), the  $M_x Ni_4 Mn_{12}O_{32}$  supercell was relaxed for integer values of x within the range of x = 1 to  $xn \ge 8$  (i.e., the number of adsorbed ions multiplied by a single ion's valency equaled or exceeded eight). This was performed for M = Li, Na, Mg, Ca, Al. Adsorption energies for each ion concentration were found using site testing by varying the position of the most recently added ion, performing a relaxation at each unique available adsorption site. To normalize the starting position, all ions were placed directly above their adsorption site, 3 Å away from the cathode. Site testing was done with a reduced k-mesh and energy cutoff of  $1 \times 1 \times 1$  and 500 eV, respectively, as these values gave the same relative energy rankings for sites at x = 1 as those found using the convergence criteria specified above. The lowest-energy configuration identified via site testing was relaxed with higher accuracy to obtain the final energy used in the voltage profile. It was ensured that all points fit on a convex hull constructed relative to the starting and ending ion concentrations.

The nudged elastic band (NEB) method [30] was used to estimate energy barriers for ion diffusion. The starting and ending points for NEB calculations were taken to be the lowest energy site found through adsorption site testing. All unique paths were sampled using five intermediate images. Density of states (DOS) were calculated and Bader charge analysis [31,32] was conducted on a  $M\mathrm{Ni_4Mn_{12}O_{32}}$  system (M = Li, Na, Mg, Ca, Al), a  $2 \times 2 \times 1$  supercell of the unit cell shown in Fig. 1. Unlike the aforementioned calculations, these final calculations included spin polarization because they pertained to electronic structure, wherein the lowest-energy spin configuration was chosen by ranging the difference in the count of spin up vs. spin down electrons from 0 to 36 (the maximum difference possible) for the first adsorbed ion and the empty structure, the results of which are reported in Supporting Information Table S1. The lowest-energy spin configuration was used for both DOS plots and Bader charge analysis. Such testing would be prohibitive for the voltage profile and was thus omitted from those calculations.

Material stability calculations were performed using a variety of the conditions described above. A convex hull for the bare cathode was constructed by relaxing  $MnO_2$ ,  $Ni_{0.25}Mn_{0.75}O_2$ , and  $NiO_2$  supercells with spin polarization. Default spin configurations were utilized for the endpoint materials due to their decreased electronic complexity.

A second convex hull was constructed for the fully sodiated cathode by relaxing Na $_{0.5}$ MnO $_2$ , Na $_{0.5}$ Ni $_{0.25}$ Mn $_{0.75}$ O $_2$ , and Na $_{0.5}$ NiO $_2$  supercells. Spin polarization was omitted for the sodiated convex hull due to the challenges cited above. All convex hull relaxations constrained cell volume while allowing atom movement and lattice vector change. Using the same procedures, an additional seven 2D Ni $_{0.25}$ Mn $_{0.75}$ O $_2$  relaxations were performed in order to determine proper Ni ordering in the material. The seven tested Ni configurations are displayed in Fig. S1. Lastly, seven *ab initio* molecular dynamics (AIMD) simulations were performed with the 2D Ni $_{0.25}$ Mn $_{0.75}$ O $_2$  supercell to evaluate stability in 300 K increments from 300 K to 2100 K. These simulations used a timestep of 1 fs and were carried out up to and exceeding 10 ps, depending on the system. The 2D system remained intact for over 10 ps up to 600 K.

#### 3. Results

#### 3.1. Material stability

To verify the stability of 2D  $\rm Ni_{0.25}Mn_{0.75}O_2$ , convex hull plots were obtained for both the empty and fully sodiated supercell. The plots (displayed in Fig S2) show that  $\rm Na_{0.5}Ni_{0.25}Mn_{0.75}O_2$  is stable by -37 meV per formula unit (meV/f.u.) compared to  $\rm Na_{0.5}NiO_2$  and  $\rm Na_{0.5}MnO_2$ , while  $\rm Ni_{0.25}Mn_{0.75}O_2$  is metastable by +47 meV/f.u. compared to  $\rm NiO_2$  and  $\rm MnO_2$ . To further investigate Ni ordering, the supercell was relaxed with seven unique Ni configurations, as displayed in Fig. S1. The unit cell chosen in this study was the second most stable configuration, resting 17 meV/f.u. above the clustered arrangement. Although the configuration with the smallest unit cell was chosen for this study, it is likely that a combination of both structures would be present in the real material.

As an additional verification of material stability, *ab initio* molecular dynamics (AIMD) simulations were performed on the 2D Ni $_{0.25}$ Mn $_{0.75}$ O $_2$  supercell at 300 K increments from 300 K up to 2100 K. Fig. S3 displays system energy vs. time for all trajectories, indicating instability when temperature reaches and exceeds 900 K. The systems at 300 and 600 K maintain stability for over 10 ps of simulation time, providing further evidence that the cathode would maintain its structure within expected experimental temperature ranges. Further, bulk Ni $_{0.25}$ Mn $_{0.75}$ O $_2$  has been synthesized and used in an experimental secondary battery [21]. Table S2 indicates that the 2D material is only 0.1 eV/f.u. less stable than the most stable bulk polymorph, a difference that would be diminished by the matrix used to separate monolayers. Given this evidence, it is reasonable to assume that 2D Ni $_{0.25}$ Mn $_{0.75}$ O $_2$ , if adequately stabilized, should be synthesizable and long-lived under normal conditions.

#### 3.2. Voltage and morphology

As shown in Fig. 2a, it is energetically favorable for all tested ions to adsorb on  $Ni_{0.25}Mn_{0.75}O_2$ . Voltage for the monovalent ions starts at 3.4 V and stays above 2 V from x=1 to x=8 for Li, indicating fairly stable performance. Sodium displays voltages just under Li up to x=4, signifying that 2D  $Ni_{0.25}Mn_{0.75}O_2$  has potential as a Na-ion cathode.

Calcium displays voltages competitive with Li and Na. The first Ca ion is adsorbed at 2.7 V, just under the voltage of the Li and Na ions. A convex hull plot showed that only phases up to x=4 were stable for the MV ions; adding higher concentrations of ions resulted in severe lattice distortion. However, because a single adsorbed  $Ca^{2+}$  ion transfers twice as much charge as a monovalent ion, its performance is better displayed relative to the number of electrons transferred rather than ions adsorbed, as shown in Fig. 2b. Here, it is clear that Ca has a voltage profile similar to Na. This means that Ca can provide similar energy density values for fewer adsorbed ions, which may improve cyclability and decrease the impact of losing ions to side reactions. Although it has lower voltages than Ca, Mg also looks like a viable alternative ion,

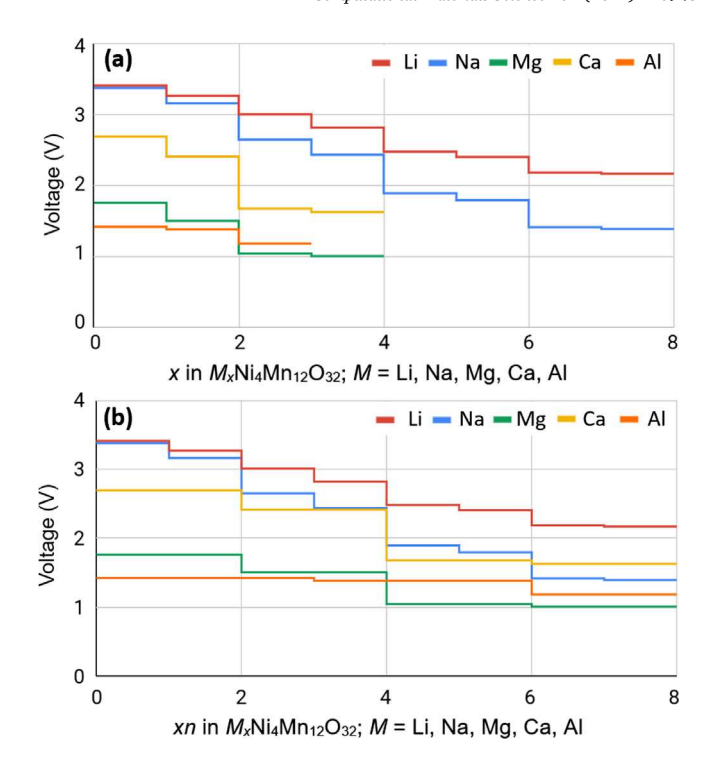


Fig. 2. Voltage profiles for adsorption of Li, Na, Mg, Ca, and Al onto 2D  $\mathrm{Ni}_{0.25}\mathrm{Mn}_{0.75}\mathrm{O}_2$  supercell relative to (a) number of ions added and (b) electrons added.

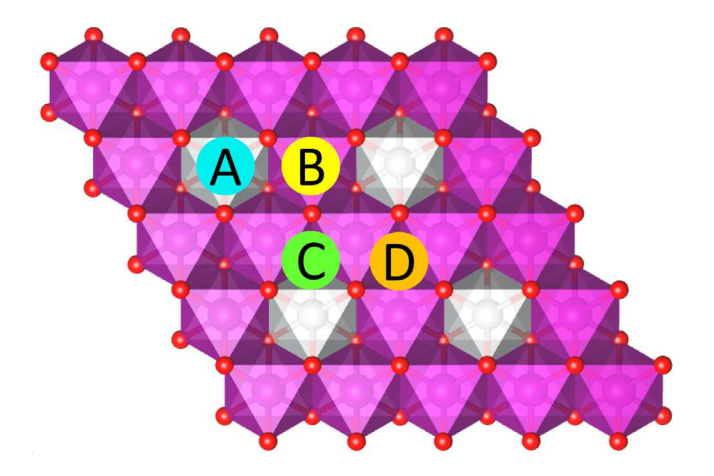


Fig. 3. Possible adsorption sites of  $Ni_{0.25}Mn_{0.75}O_2$ . The A and B sites are directly over an Ni or Mn atom, respectively, while the C and D sites are directly over an O atom. The C site is bordered by one Ni atom, while the D site is bordered only by Mn atoms.

having an initial voltage of 1.8 V and providing relatively consistent voltage through xn=4. Aluminum performed similarly, maintaining a remarkably stable voltage of 1.4 to 1.2 V through xn=8.

Aside from predicting performance, the voltage profile also unveiled adsorption patterns for each ion. Four stable adsorption sites were found, although only three proved energetically favorable in the voltage profile: directly on top of a Ni atom; a Ni-adjacent O atom; and an O atom surrounded by Mn atoms. These correspond to sites A, C, and D, respectively, in Fig. 3. Regardless of charge, it was energetically favorable for ions to alternate on which side of the 2D  $\mathrm{Ni}_{0.25}\mathrm{Mn}_{0.75}\mathrm{O}_2$  sheet they adsorbed. Both the mono- and divalent ions would adsorb on a Ni-adjacent O site for odd values of x, but for even values of x, the monovalents preferred Ni sites while the divalents tended to adsorb at Mn-surrounded O. Although its voltage profile only extended up to x=3, trivalent Al also adsorbed onto Ni sites, suggesting that odd-valence ions have a stronger interaction with Ni than even-valence

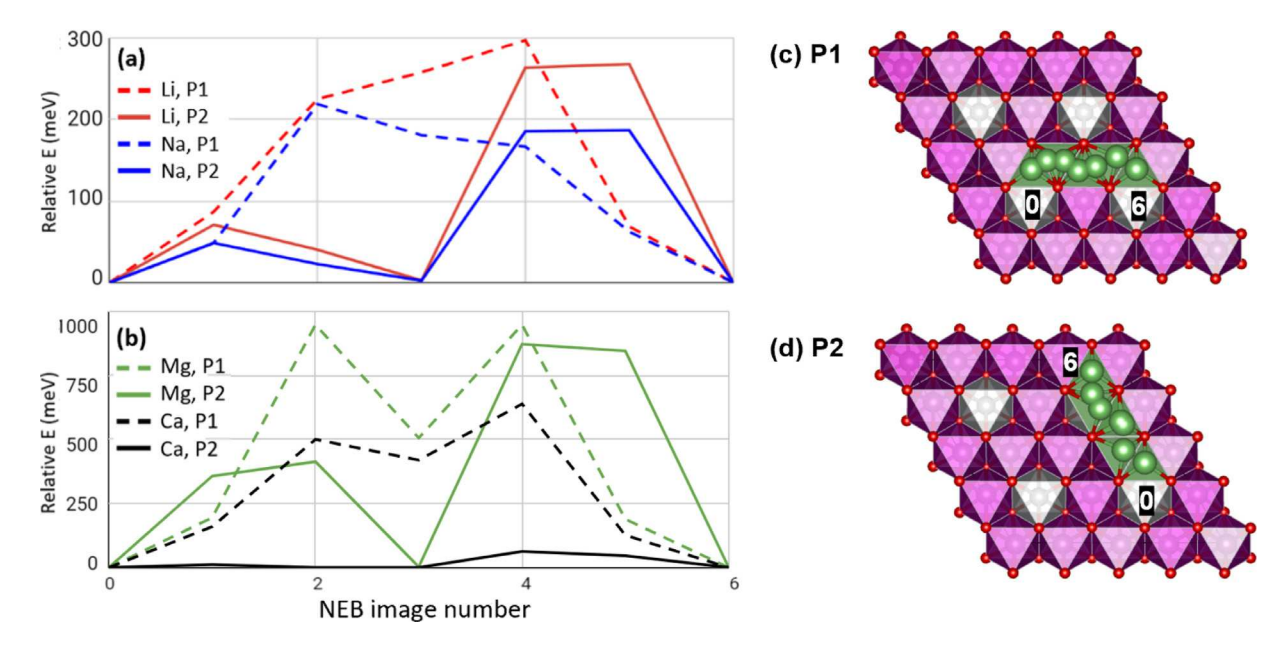


Fig. 4. Diffusion barriers for (a) monovalent and (b) divalent ions. Paths (c) P1 and (d) P2 are illustrated with the Li ion, where starting and ending positions are labeled with "0" and "6", respectively.

ions. The Al ion went so far as to partially displace Ni in the lattice, supporting the strength of its interaction with Ni and providing some evidence against using Al with this cathode. In this case, the charge density of both cathode and ion is too high for reversible adsorption; lower charge density cathodes such as sulfides, most notably  $\rm Mo_6S_8$ , have been found to be more suitable for this application [33,34]. A view of the cathode with the maximum ion concentration studied in this paper is available in Fig. S4.

Given the tendency of PBE to underestimate TMO cathode voltages, it is likely that the true voltage values are higher than reported herein [35]. Chakraborty et al. confirmed this trend for bulk LiMO2, M = Ni, Co, Mn, but their results also showed that PBE reproduces voltage trends seen with SCAN, which most consistently reproduced near-experimental voltages; thus, we believe that our calculations provide realistic estimates of the relative performance of each system [36]. Although experimental data for 2D Ni<sub>0.25</sub>Mn<sub>0.75</sub>O<sub>2</sub> is not available for direct benchmarking, previous work from our group employing PBE has shown excellent agreement with experiment [37,38]. This agreement suggests that PBE may provide accurate voltage values as well as qualitative trends between ions. A similar discussion may be had regarding spin polarization. Supporting Information Table S3 shows that in the majority of cases, the omission of spin polarization increased voltage values by approximately 10%-20% for the first adsorbed ion in the system. The only exception is Al, which resulted in a 5.5% decrease in voltage, but this ion adsorbs in a much more invasive manner than the others, perhaps leading to this deviation. Regardless, relative voltage trends between ions are preserved, suggesting that while spin polarization may change absolute voltage values, profile trends are conserved.

### 3.3. Diffusion barriers

Poor diffusion kinetics comprise one of the limiting factors in MVIB cathodes, so it is important to check for prohibitively high barriers among the five ions adsorbed onto 2D  $\mathrm{Ni_{0.25}Mn_{0.75}O_2}$ . Although plating, stripping, and other ion transfer processes are also relevant to the function of the cathode, we report only on lateral surface diffusion. This would likely be the dominant mode of ion motion within the cathode, as it is energetically favorable for ions to adsorb and remain adsorbed onto the  $\mathrm{Ni_{0.25}Mn_{0.75}O_2}$  monolayer, meaning that any diffusion to accommodate higher ion concentrations on the oxide surface would

feature lateral movement without plating/stripping. As summarized in Fig. 4, Li, Na, and Ca have low diffusion barriers of 267, 187, and 63 meV, respectively, while that of Mg is much higher at 873 meV. Consequently, Li, Na, and Ca ions would be able to reversibly adsorb onto the 2D  $\rm Ni_{0.25}Mn_{0.75}O_2$  sheets as the cathode is cycled, but the Mg diffusion barrier may be too high to allow for its timely diffusion, signifying incompatibility with the material. The NEB calculation to obtain the Al diffusion barrier was attempted but failed due to the ion embedding into the material (see Fig. S5); it can be assumed that the barrier is too high for room temperature diffusion due to this behavior.

Ion size appears to be a determining factor of diffusion barriers in Fig. 4. For a given diffusion path, Na has a lower diffusion barrier than Li, and Ca has a lower barrier than Mg. This indicates that larger ion size, and consequent increased adsorption distance, reduce the Coulombic interaction between the ion and the host material. This agrees with the findings by Leong et al. where a similar trend was observed between Li and Na ions adsorbed onto 2D TMOs [11]. With the exception of Al, all ions could diffuse via two paths, either traveling across only Mn atoms or a mix of Ni and Mn atoms. These are labeled as P1 and P2 in Fig. 4d and are referred to as the Mn and Ni paths, respectively. Where given the choice, the Ni path was found to be favorable, indicating a stabilizing interaction between Li/Na/Ca/Mg and Ni. This agrees with adsorption trends described above, wherein ions preferentially interact with Ni. NEB images for Li are provided in Fig. 4, while those for Na, Ca, and Mg are shown in Fig. S6.

#### 3.4. Electronic structure

A successful cathode should have sufficient electronic conductivity to facilitate ion intercalation or adsorption. This trait was verified in monolayer  $\mathrm{Ni_{0.25}Mn_{0.75}O_2}$  by plotting the DOS for the cathode with each adsorbed ion as well as the bare material using the PBE functional. Fig. 5 suggests that pure, monolayer  $\mathrm{Ni_{0.25}Mn_{0.75}O_2}$  is semiconducting, which is undesirable for a material that needs to accommodate continuous electron transport. However, the pristine state is not representative of experimental conditions, where some metal ions are always present in the cathode, even when the cell is fully charged. Thus, we also investigate the DOS for the cathode with adsorbed ions at small concentrations to predict the conductivity of 2D  $\mathrm{Ni_{0.25}Mn_{0.75}O_2}$  in a secondary ion battery context. Here, Fig. 5 shows much more promising results. Upon adsorption of even small amounts of ions (0.063 per formula

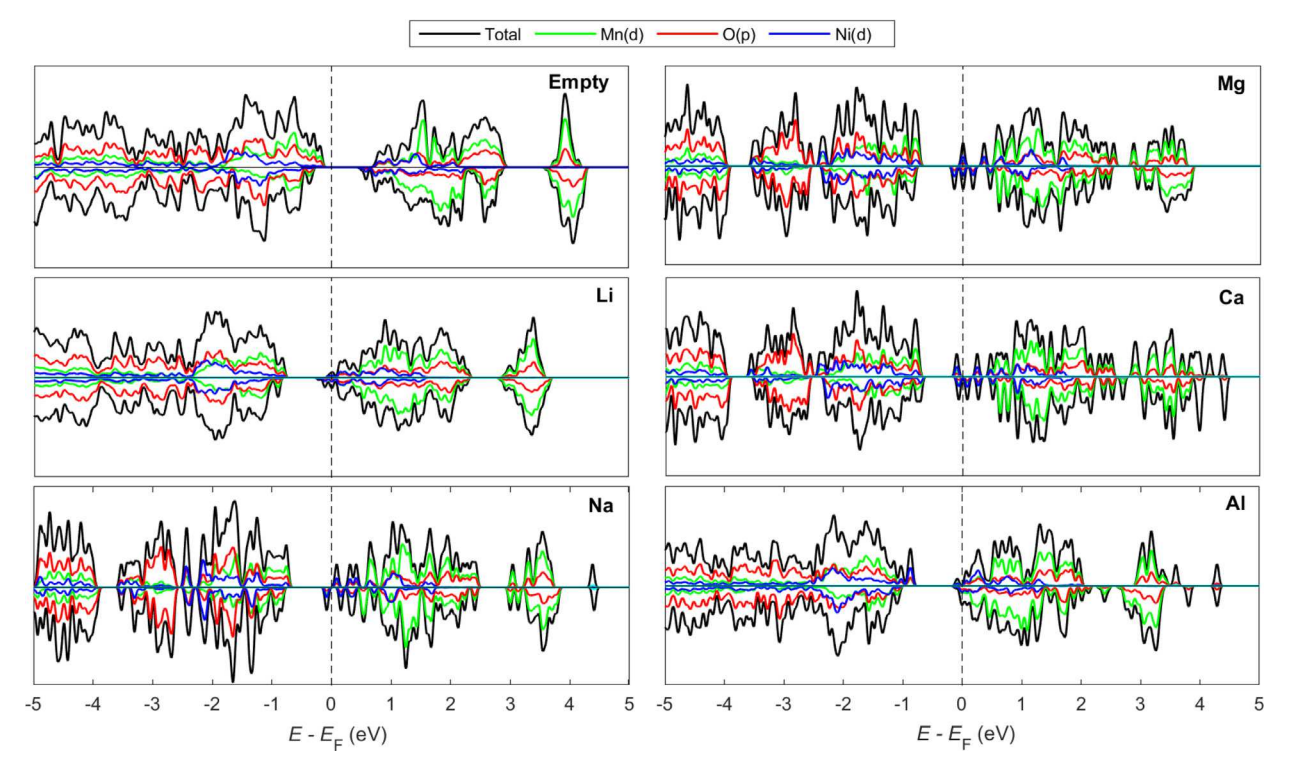


Fig. 5. Spin-polarized density of states for  $M_{0.0625}Ni_{0.25}Mn_{0.75}O_2$ .

unit), 2D Ni<sub>0.25</sub>Mn<sub>0.75</sub>O<sub>2</sub> becomes metallic. As can be seen in the Li and Na plots in Fig. 5, adding a single extra electron to the system shifts the Fermi energy up to the former conduction band, making the material much more receptive to further electronic conduction. Thus, as it exists in real-world applications, 2D  $Ni_{0.25}Mn_{0.75}O_2$  is likely to be electronically conductive, possibly explaining the experimental increase in conductivity experienced by MnO2 upon addition of metal dopants [18]. To verify that these conclusions were not merely an artifact of the selected functional, DOS was plotted for both the pure and sodiated structure using a variety of GGAs and meta-GGAs. PBE alone is known to yield overly-delocalized systems in TMOs, so it is necessary to benchmark it against higher-level functionals [35]. In addition to the PBE GGA, we tested PBE-D3, which accounts for dispersion forces relevant to adsorption [39]; PBE+U, which allows for increased electron localization, as seen in TMOs [40]; and the SCAN meta-GGA, which accounts for short and medium-range van der Waals interactions [41]. All tested functionals resulted in a metallic transition upon the addition of a Na ion, as can be seen in Supporting Information Fig. S7. Thus, we propose that PBE is adequate for a qualitative analysis of electronic structure under the conditions used in our simulation. We expect these observations to extend to the other ions because of the similarities found in the band gap behavior using PBE.

Examining the DOS also reveals which atoms play the biggest role in the conductivity of 2D  $\mathrm{Ni_{0.25}Mn_{0.75}O_2}$ . Shown in the adsorption of the monovalent ions in Fig. 5, it appears that the first electron is added to hybridized states made up of the p orbitals of O and d orbitals of Mn and Ni. All three atoms have similar partial density of states (PDOS) values near the Fermi level; however, given the small concentration of Ni relative to Mn and O, Ni accommodates a disproportionately large amount of the added charge, suggesting that Ni plays a significant role in the conduction of the material. A similar argument may be made for Mn relative to O, although the difference in concentration is not as large as with Ni. Unlike Mn, Ni assists with conductivity by decreasing the band gap of surrounding atoms. Fig. S8 displays this effect by plotting the PDOS of oxygen atoms in  $\mathrm{MnO_2}$  vs.  $\mathrm{Ni_{0.25}Mn_{0.75}O_2}$ , then plotting PDOS of individual atoms in  $\mathrm{Ni_{0.25}Mn_{0.75}O_2}$ , showing that oxygen atoms closer to Ni have a smaller band gap.

This pattern persists for the divalent ions, Mg and Ca. There are now two electrons being added to the system, as seen in the peaks just below the Fermi level in the plots for Mg and Ca in Fig. 5. The gap between the former valence band and the conduction band decreases as compared to that of the monovalent ions, suggesting that a broader range of energy values are now occupied and that the added electrons are in a more favorable position. Once again, Ni disproportionately accommodates the new electrons, followed by Mn and O. The trivalent ion, Al, follows a similar pattern, although its DOS does not show three distinct peaks; this may be because they are too close and instead merge into a single peak.

While the DOS shows which orbitals additional electrons occupy, Bader charge analysis can show which particular atoms accommodate these electrons. Each ion (Li, Na, Mg, Ca, Al) was adsorbed at a concentration of M<sub>0.0625</sub>Ni<sub>0.25</sub>Mn<sub>0.75</sub>O<sub>2</sub> then examined through Bader charge analysis, which was accompanied by a charge density difference distribution plot (Fig. 6). The results summarized in Table 1 show that the electrons accompanying the adsorbed ion are mostly distributed throughout the cathode material, but a significant amount remain near the ion. Contrary to electron affinity trends, smaller ions adopt a more positive charge than larger ions when normalized for valence. For all ions, it seems like oxygen accepts most of the new electrons, followed by Ni, as seen in Table 1. Both of these facts can be seen visually in the charge density difference distributions (Fig. 6), where there is a distinct area of depleted charge around the adsorbed ion and an area of excess charge around oxygen atoms, especially those closest to the adsorbed ion. A review of individual atom charges for the CaNi<sub>4</sub>Mn<sub>12</sub>O<sub>32</sub> supercell supported the conclusions of the average element charges presented in Table 1 and the charge density difference of Fig. 6. Most atoms (including all Ni and Mn) underwent a change in charge between 0.01e and -0.08e, while the oxygen atoms close to the Ca ion experienced charge transfer between -0.21e and -0.24e.

Surprisingly, Bader charge analysis does not support the conclusion drawn from the DOS that Ni and Mn are disproportionately responsible for accommodating the new electrons introduced by the ion. If this were the case, one would expect these metals to have a more negative change

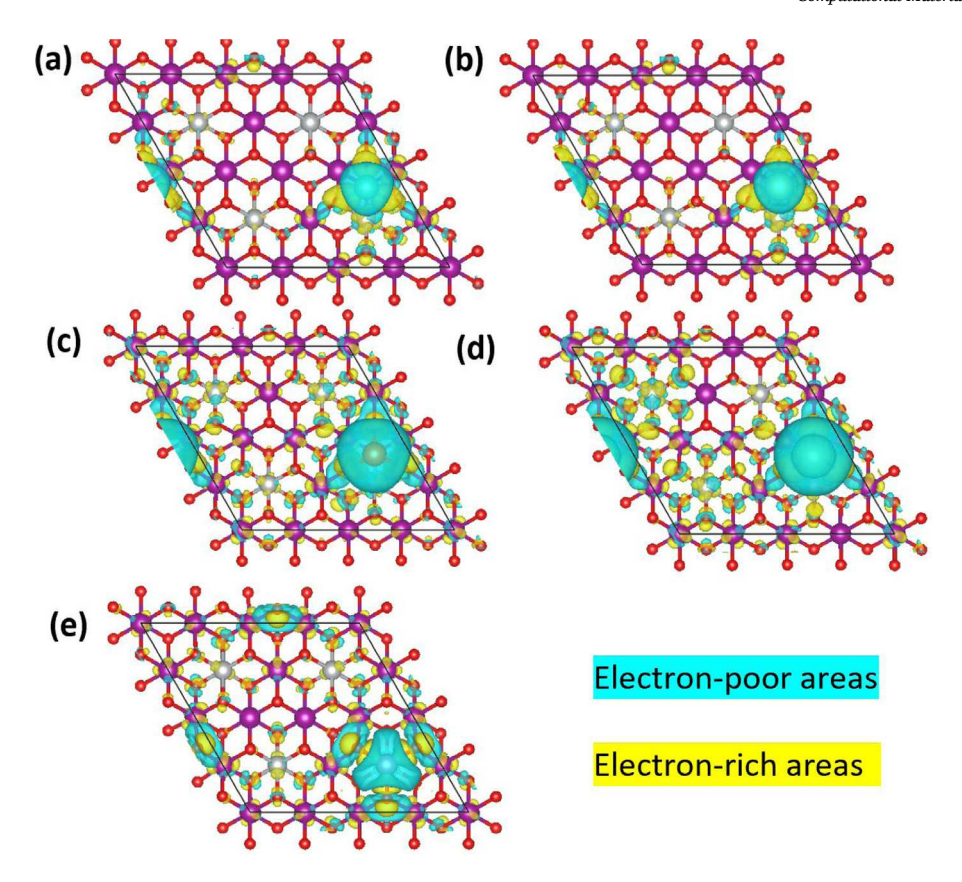


Fig. 6. Charge density difference plots for  $M_{0.0625}Ni_{0.25}Mn_{0.75}O_2$  vs. bare 2D  $Ni_{0.25}Mn_{0.75}O_2$ , where M=(a) Na, (b) Li, (c) Ca, (d) Mg, (e) Al. A blue surface indicates an electron-deficient (positive) area, while a yellow one indicates an electron-rich (negative) area. (For interpretation of the references to color in this figure legend, the reader is referred to the web version of this article.)

Table 1 Average charges on each type of element of monolayer  $M_{0.0625}\mathrm{Ni_{0.25}Mn_{0.75}O_2}$  after adsorption of Li, Na, Mg, Ca, and Al. The final three columns display the change in charge relative to the bare cathode.

	Total Bader charge (e)				Change in charge (e)			
M	Ion	Ni	Mn	0	Ni	Mn	0	
Na	0.891	1.305	1.682	-0.822	-0.019	-0.004	-0.024	
Li	0.899	1.306	1.683	-0.822	-0.019	-0.004	-0.024	
Ca	1.623	1.283	1.673	-0.839	-0.040	-0.013	-0.041	
Mg	1.689	1.283	1.675	-0.841	-0.042	-0.012	-0.043	
Al	2.398	1.249	1.682	-0.862	-0.075	-0.005	-0.064	

in charge than oxygen, but this does not occur. This highlights the value of both plotting DOS and performing Bader charge analysis, as each method has its own merits and limitations. As with oxygen, Mn and Ni atoms closer to the adsorbed ion have more electrons than those far from the adsorbed ion. Notably, in the case of Al, the Ni atom displaced by Al gains a significant amount of negative charge (0.23*e*), contrasting with the general trend of very mild oxidation. These changes in charge are too localized to be shown meaningfully in Fig. 6, but are clearly shown in Table 1.

However, other insights may be inferred from the charge density difference distributions in Fig. 6, chief among them being the confirmation of adsorption as opposed to a conversion reaction. In the presence of a conversion reaction, the adsorption of an ion leads to the formation of two heterogeneous compounds rather than a single-phase product. Were this the case, one would expect a decreased charge density in the bonds between atoms close to the adsorbed ion and their neighbors, indicative of weakening bonds between the conversion products. There is no evidence of this with the monovalent ions of Li and Na (Fig. 6 a and b, respectively), possibly meaning that they will be less prone

to conversion reactions. Once valence increases, as with divalent Mg and Ca and trivalent Al, a distinct area of decreased charge density appears between the oxygens closest to the ion and their neighboring Mn atoms (Fig. 6 c and d, respectively), agreeing with the general trend that MV ions are more prone to oxide conversion reactions [2]. This is corroborated by the morphology of the cathode, which shows significant distortion of the divalent systems at around x = 6. Although they show increased polarization, these results do not rule out the possibility of a 2D Ni<sub>0.25</sub>Mn<sub>0.75</sub>O<sub>2</sub> multivalent ion cathode system.

#### 4. Discussion

Prior to analyzing the above results, it is necessary to acknowledge the limitations of our study, particularly the unknown effects that true experimental conditions may have on the performance of 2D Ni<sub>0.25</sub>Mn<sub>0.75</sub>O<sub>2</sub>. Most significantly, both the electrolyte and the matrix or solvent used to separate monolayers are absent in the present work. While Imandi et al. found that the inclusion of solvation decreased the diffusion barrier of an Ag adatom on Ag(001) surface from 525 to 297 meV [42], it is not known if these results are transferable to the current system. We may speculate that solvent presence at the 2D Ni<sub>0.25</sub>Mn<sub>0.75</sub>O<sub>2</sub> surface would change the diffusion barrier by several hundred meV, but any increased precision requires further investigation. The effect of layer-separating compounds is similarly opaque. Relative to bulk, any compound that separates cathode layers generally improves transport properties and capacity, but it is difficult to distinguish the impact of the compound from the impact of decreased interlayer interaction [43,44]. The effects of local environment on voltage are even less predictable, as they involve the system-specific energetics of changing solvent orientations, raising compelling questions for future investigation [45]. With these limitations in mind, it is possible to analyze the significance of our results.

**Table 2** PBE-calculated voltages (V) and diffusion barriers (meV) for Li and Na ions on monolayer (2D) TMOs and TMDs. All sources calculate voltage with an ion concentration of 0.125 (corresponding to x = 2 in Fig. 2a) except Ref. [10], which substitutes 0.667. Diffusion barriers are calculated with an ion concentration of 0.063, 0.125, and 0.667 for our original data, Ref. [11], and Ref. [10], respectively. The first column of data is from the present work.

				M = Li					
	$\mathrm{Ni_{0.25}Mn_{0.75}O_{2}}$	$\mathrm{MnO}_2$	$\mathrm{CoO}_2$	${ m NiO}_2$	$\mathrm{MoO}_2$	$\mathrm{WO}_2$	${\rm VS}_2$	$MoS_2$	$\mathrm{WS}_2$
Voltage Barrier	3.34 267	2.55 [11]-3.54 [10] 148 [10]-156 [11]	3.56 [11] 180 [11]	2.72 [11] 186 [11]	2.16 [10] 95 [10]	1.4 [10] 122 [10]	0.18 [10] 208 [10]	0.96 [10] 216 [10]	0.88 [10] 220 [10]
Burrier	207	110 [10] 100 [11]	100 [11]	M = Na	30 [10]	122 [10]	200 [10]	210 [10]	220 [10]
Voltage	3.27	2.4 [11]	3.4 [11]	2.6 [11]	_	_	-	_	_
Barrier	187	121 [11]	122 [11]	129 [11]	-	-	-	-	-

**Table 3** PBE-calculated voltages V and diffusion barriers D (meV) for Na, Li, Ca, Mg, and Al paired with bulk, layered MnO $_2$  and compared to 2D Ni $_{0.25}$ Mn $_{0.75}$ O $_2$ . Ion concentrations are noted in column headings with the exception of  $V_{\rm end}$ , where concentration is listed in the entry's subscript.

	2D	$M_x \text{Ni}_{0.25} \text{Mn}_0$	3D <i>M</i>	$3D M_x MnO_2$		
M	$V_{x=0.063}$	$V_{\mathrm{end}}$	D	$V_{x=0.5}$	D	
Na	3.38	$2.27_{0.5}$	187	-	-	
Li	3.42	$2.72_{0.5}$	267	3.03 [5]	-	
Ca	2.70	$2.10_{0.25}$	63	2.7 [5]	550 [ <b>5</b> ]	
Mg	1.76	$1.33_{0.25}$	873	1.95 [5]	-	
Al	1.42	$1.33_{0.188}$	-	1.53 [5]	-	

2D  $\mathrm{Ni}_{0.25}\mathrm{Mn}_{0.75}\mathrm{O}_2$  compares favorably both with 2D transition-metal chalcogenides (TMCs) and similar bulk layered cathodes reported in the literature. Variations in computational methods and a dearth of data make it difficult to draw direct comparisons between studies, but the data is sufficient for analyzing the relative performance of the cathodes. The most significant discrepancy is in the ion concentration used to calculate voltage and diffusion barriers; this ranged anywhere from 0.063 to 0.667 ions per unit cell. Further, some voltages were originally reported as adsorption energies, which had to be converted to voltage using an adapted version of Eq. (2). With this in mind, one can still glean where 2D  $\mathrm{Ni}_{0.25}\mathrm{Mn}_{0.75}\mathrm{O}_2$  stands in comparison with other TMCs.

Table 2 summarizes voltage and diffusion barrier data for Li- and Na-ion monolayer TMCs. At 3.34 V, 2D Ni<sub>0.25</sub>Mn<sub>0.75</sub>O<sub>2</sub> is in the upper rungs of performance of 2D Li-ion TMOs, which range anywhere from 2-3.5 V. In fact, it is almost on par with CoO<sub>2</sub> and the upper range for MnO2; however, it must be noted that at the specified concentrations, Leong et al. [11] only adsorbed ions on one side of a monolayer, while the other sources had ions on both sides. As it is energetically preferable to spread out ions, the voltages calculated by Leong et al. [11] may be deceptively low, suggesting that the voltage for MnO2 is closer to 3.54 V and that the voltages for  $CoO_2$  and  $NiO_2$  are higher than reported. Thus, it is fairly certain that CoO2 still provides the highest voltage of the reported oxides. While CoO2 out-performs all considered materials in both voltage and diffusion barrier, the humanitarian and economic issues associated with Co discourage its use as a cathode material, necessitating the alternatives discussed herein. It is possible that adding Ni to MnO2 has improved upon its voltage properties (as suggested by the increase in voltage from MnO<sub>2</sub> to NiO<sub>2</sub> in Ref. [11]), but there is too much computational variability to draw a conclusion from the numbers alone. Although voltage results are favorable, 2D  $Ni_{0.25}Mn_{0.75}O_2$  has a diffusion barrier of 267 meV, above  $MnO_2$  (148– 156 meV) and NiO<sub>2</sub> (186 meV). However, such barriers are permissive for room-temperature operation, meaning that 2D Ni<sub>0.25</sub>Mn<sub>0.75</sub>O<sub>2</sub> is still competitive.

The increase in voltage upon the addition of Ni to  $MnO_2$  can be explained by the ions' increased interaction with Ni atoms. As stated in the Electronic structure section, the additional charge accompanying adsorbed ions is disproportionately placed onto Ni atoms. Further,

diffusion paths above the Ni atom have lower energy barriers than those avoiding it. Both of these results indicate that ions preferentially interact with Ni, which may cause adsorption to be more energetically favorable on a  $Ni_{0.25}Mn_{0.75}O_2$  sheet when compared to pure 2D  $MnO_2$ . This trend also agrees with the higher voltage of  $Li_{0.125}NiO_2$  relative to  $Li_{0.125}MnO_2$  [11]. It is possible that superior  $MnO_2$  dopants exist, but their stability under electrochemical intercalation is not as certain as that of an experimentally verified material. Additionally,  $NiO_2$  has also been shown to have higher voltages than  $MnO_2$ , meaning that Ni doping has the possibility of improving voltage without compromising costs, which is not true of all conductive additives [11]. However, Ni concentrations must be carefully controlled, as high Ni concentrations have been connected to thermal instability in cathodes such as  $LiNi_xCo_yMn_zO_2$  [19].

Li-ion 2D TMOs are promising, but TMDs leave something to be desired. TMD voltages reported in Table 2 are less than half those of TMOs, while the diffusion barriers are almost twice as high. These may deserve consideration as alternatives to TMOs if they have superior interfacial properties, but the reported metrics inspire more confidence in TMOs overall. As selenides generally have even lower voltages [46], oxygen seems to be the choice chalcogen for battery cathodes.

As a 2D Na-ion cathode,  $Ni_{0.25}Mn_{0.75}O_2$  follows trends found in Ref. [11]; that is, that both voltage and diffusion barriers are decreased relative to Li. Considering the scarcity of Li, losses in voltage may be worth the improved accessibility and diffusion properties of Na.

When compared to bulk oxides, 2D Ni<sub>0.25</sub>Mn<sub>0.75</sub>O<sub>2</sub> provides improved diffusion properties, but reduced energetics. The computed average voltage of 2.27 V for 2D Na<sub>0.5</sub>Ni<sub>0.25</sub>Mn<sub>0.75</sub>O<sub>2</sub> is far lower than the experimental average voltage of 3.5 V for bulk Na<sub>0.5</sub>Ni<sub>0.25</sub>Mn<sub>0.75</sub>O<sub>2</sub> [21], uncovering drawbacks not seen with the low-concentration computed value. While there is no direct computational comparison available for bulk Ni<sub>0,25</sub>Mn<sub>0,75</sub>O<sub>2</sub>, data are available for Li, Mg, Ca, or Al when paired with layered 3D  $\mathrm{MnO}_2$  (summarized in Table 3). As before, there is a significant decrease in voltage in the 2D system relative to bulk MnO<sub>2</sub>. The computed voltage difference between the systems is likely higher than reported in Table 3 for Ca, Mg, and Al, as the endpoint concentration of these ions adsorbed on 2D Ni<sub>0.25</sub>Mn<sub>0.75</sub>O<sub>2</sub> was less than half that used with MnO2. However, these losses may be recuperated through improved diffusion kinetics in the monolayer. As this is observed with Ca - the diffusion barrier decreases from 550 meV to 63 meV - this is a probable occurrence for the remaining ions. The value of this trade-off may be determined based on desired battery operating conditions and the chosen ion.

# 5. Conclusion

Our calculations predict that monolayer  $\mathrm{Ni}_{0.25}\mathrm{Mn}_{0.75}\mathrm{O}_2$  performs on par with the best Co-free 2D TMOs, maintaining satisfactory voltage values and diffusion barriers that allow for room temperature operation when paired with Li, Na, and Ca. Consistent with literature, employing a 2D system enhances ionic conductivity [8–10], overcoming a common challenge in multivalent ion batteries. Experimental work is needed to confirm whether the addition of Ni improves upon the poor electronic

conductivity of monolayer MnO2, although the DOS plots suggest that adsorbing even small concentrations of ions transforms the material from a semiconductor to a conductor. Due to its adequate voltages, low diffusion barriers, and likely conductivity, 2D  $\mathrm{Ni}_{0.25}\mathrm{Mn}_{0.75}\mathrm{O}_2$  seems like a promising candidate as a Li, Na, or Ca-ion 2D battery cathode. Meanwhile, poor diffusion barriers and low average voltages suggest that 2D Ni<sub>0.25</sub>Mn<sub>0.75</sub>O<sub>2</sub> would perform suboptimally with Mg and Al. This is likely because Mg is too small when compared with Ca, coming too close to the monolayer and interacting too strongly, leading to a prohibitively high diffusion barrier. Similarly, Al seems to interact too strongly with Ni, likely causing insufficient Al-ion conductivity. Beyond confirming electronic conductivity, experimentation is necessary to find an effective method of isolating Ni<sub>0.25</sub>Mn<sub>0.75</sub>O<sub>2</sub> layers as well as a compatible electrolyte and anode. In the face of increasing scarcity of traditional Li-ion cathode constituents, 2D Ni<sub>0.25</sub>Mn<sub>0.75</sub>O<sub>2</sub> is a promising alternative.

#### CRediT authorship contribution statement

**Diana Liepinya:** Methodology, Validation, Formal analysis, Investigation, Data curation, Writing – original draft, Writing – review & editing, Visualization. **Robert Shepard:** Conceptualization, Methodology, Formal analysis, Writing – review & editing, Supervision. **Manuel Smeu:** Conceptualization, Validation, Formal analysis, Resources, Writing – review & editing, Supervision, Project administration, Funding acquisition.

#### Declaration of competing interest

The authors declare that they have no known competing financial interests or personal relationships that could have appeared to influence the work reported in this paper.

#### Acknowledgments

This work was supported by the National Science Foundation Research Experiences for Undergraduates Program (DMR-1950555) and Binghamton University's Transdisciplinary Area of Excellence in Smart Energy, USA. DFT calculations were performed on the Spiedie cluster at Binghamton University, the Extreme Science and Engineering Discovery Environment (XSEDE, supported by NSF Grant No. ACI-1053575) under allocation TG-DMR180009, and the CARBON cluster at the Center for Nanoscale Materials (Argonne National Laboratory, supported by the U.S. DOE, Office of Basic Energy Sciences (BES), DE-AC02-06CH11357) under allocation CNM72207.

## Appendix A. Supplementary data

Supplementary material related to this article can be found online at <a href="https://doi.org/10.1016/j.commatsci.2021.110948">https://doi.org/10.1016/j.commatsci.2021.110948</a>. This includes figures and tables regarding electronic structure, stability, and adsorption behavior.

# References

- I. Tsiropoulos, N. Lebedeva, Li-ion Batteries for Mobility and Stationary Storage Applications, Joint Research Centre, 2018, p. 3.
- [2] P. Canepa, G. Sai Gautam, D.C. Hannah, R. Malik, M. Liu, K.G. Gallagher, K.A. Persson, G. Ceder, Odyssey of multivalent cathode materials: Open questions and future challenges, Chem. Rev. 117 (5) (2017) 4287–4341.
- [3] B. Weiss, O. Michiyo, Environmental Risk Mitigation: Coaxing a Market in the Battery and Energy Supply and Storage Industry, Springer International Publishing, Cham, Switzerland, 2016.
- [4] J. Wu, Q. Yang, J. Li, L. Zhong, L. Dong, W. Liu, J. Mou, C. Xu, Origin of storage capacity enhancement by replacing univalent ion with multivalent ion for energy storage, Electrochim. Acta 282 (2018) 30–37.
- [5] T.R. Juran, J. Young, M. Smeu, Density functional theory modeling of MnO2 polymorphs as cathodes for multivalent ion batteries, J. Phys. Chem. C 122 (16) (2018) 8788–8795.

- [6] T.S. Arthur, R. Zhang, C. Ling, P.-A. Glans, X. Fan, J. Guo, F. Mizuno, Understanding the electrochemical mechanism of K-αMnO2 for magnesium battery cathodes, ACS Appl. Mater. Interfaces 6 (10) (2014) 7004–7008.
- [7] L. Dong, W. Yang, W. Yang, Y. Li, W. Wu, G. Wang, Multivalent metal ion hybrid capacitors: A review with a focus on zinc-ion hybrid capacitors, J. Mater. Chem. A 7 (23) (2019) 13810–13832.
- [8] L. Peng, Y. Zhu, X. Peng, Z. Fang, W. Chu, Y. Wang, Y. Xie, Y. Li, J.J. Cha, G. Yu, Effective interlayer engineering of two-dimensional VOPO4 nanosheets via controlled organic intercalation for improving alkali ion storage, Nano Lett. 17 (10) (2017) 6273–6279.
- [9] P. Xiong, R. Ma, N. Sakai, X. Bai, S. Li, T. Sasaki, Redox active cation intercalation/deintercalation in two-dimensional layered MnO2 nanostructures for high-rate electrochemical energy storage, ACS Appl. Mater. Interfaces 9 (2017) 6282–6291.
- [10] S. Deng, L. Wang, T. Hou, Y. Li, Two-dimensional MnO2 as a better cathode material for lithium ion batteries, J. Phys. Chem. C 119 (52) (2015) 28783–28788.
- [11] C.C. Leong, H. Pan, S.K. Ho, Two-dimensional transition-metal oxide monolayers as cathode materials for Li and Na ion batteries, Phys. Chem. Chem. Phys. 18 (10) (2016) 7527–7534.
- [12] Y. Zhou, C. Geng, A MoO2 sheet as a promising electrode material: Ultrafast li-diffusion and astonishing Li-storage capacity, Nanotechnology 28 (10) (2017) 105402
- [13] K.S. Chen, I. Balla, N.S. Luu, M.C. Hersam, Emerging opportunities for twodimensional materials in lithium-ion batteries, ACS Energy Lett. 2 (9) (2017) 2026–2034.
- [14] M.S. Stark, K.L. Kuntz, S.J. Martens, S.C. Warren, Intercalation of layered materials from bulk to 2D, Adv. Mater. 31 (27) (2019) 1808213.
- [15] K. Kalantar-zadeh, J.Z. Ou, T. Daeneke, A. Mitchell, T. Sasaki, M.S. Fuhrer, Two dimensional and layered transition metal oxides, App. Mater. Today 5 (2016) 73–89.
- [16] D. Jia, X. Chen, H. Tan, F. Liu, L. Yue, Y. Zheng, X. Cao, C. Li, Y. Sun, H. Liu, J. Liu, Boosting electrochemistry of manganese oxide nanosheets by ostwald ripening during reduction for fiber electrochemical energy storage device, ACS Appl. Mater. Interfaces 10 (36) (2018) 30388–30399.
- [17] A.L.M. Reddy, M.M. Shaijumon, S.R. Gowda, P.M. Ajayan, Coaxial MnO2/carbon nanotube array electrodes for high-performance lithium batteries, Nano Lett. 9 (3) (2009) 1002–1006.
- [18] J. Kang, A. Hirata, L. Kang, X. Zhang, Y. Hou, L. Chen, C. Li, T. Fujita, K. Akagi, M. Chen, Enhanced supercapacitor performance of MnO2 by atomic doping, Angew. Chem. Int. Ed. 52 (6) (2013) 1664–1667.
- [19] H.J. Noh, S. Youn, C.S. Yoon, Y.K. Sun, Comparison of the structural and electrochemical properties of layered Li[NixCoyMnz]O2 (x=1/3, 0.5, 0.6, 0.7, 0.8 and 0.85) cathode material for lithium-ion batteries, J. Power Sources 233 (2013) 121–130.
- [20] Z. Ye, T. Li, G. Ma, Y. Dong, X. Zhou, Metal-ion (Fe, V, Co, and Ni)-doped MnO2 ultrathin nanosheets supported on carbon fiber paper for the oxygen evolution reaction, Adv. Funct. Mater. 27 (44) (2017) 1704083.
- [21] Q. Li, Y. Qiao, S. Guo, K. Jiang, Q. Li, J. Wu, H. Zhou, Both cationic and anionic co-(de)intercalation into a metal-oxide material, Joule 2 (6) (2018) 1134–1145.
- [22] K. Saravanan, A. Jarry, R. Kostecki, G. Chen, A study of roomerature LixMn1.5Ni0.5O4 solid solutions, Sci. Rep. 5 (111) (2015) 1–11.
- [23] H. Arai, K. Sato, Y. Orikasa, H. Murayama, I. Takahashi, Y. Koyama, Y. Uchimoto, Z. Ogumi, Phase transition kinetics of LiNi0.5Mn1.5O 4 electrodes studied by in situ X-ray absorption near-edge structure and X-ray diffraction analysis, J. Mater. Chem. A 1 (35) (2013) 10442–10449.
- [24] G. Kresse, J. Hafner, Ab initio molecular dynamics for liquid metals, Phys. Rev. B 47 (1) (1993) 558-561.
- [25] G. Kresse, J. Furthmüller, Efficient iterative schemes for ab initio total-energy calculations using a plane-wave basis set, Phys. Rev. B 54 (16) (1996) 11169–11186.
- [26] G. Kresse, J. Hafner, Ab initio molecular-dynamics simulation of the liquid-metalamorphous- semiconductor transition in germanium, Phys. Rev. B 49 (20) (1994) 14251–14269.
- [27] P. Blöchl, Projector augmented-wave method, Phys. Rev. B 50 (24) (1994) 17953–17979.
- [28] J.P. Perdew, K. Burke, M. Ernzerhof, Generalized gradient approximation made simple, Phys. Rev. Lett. 77 (18) (1996) 3865–3868.
- [29] K. Momma, F. Izumi, VESTA 3 for three-dimensional visualization of crystal, volumetric and morphology data, J. Appl. Cryst. 44 (6) (2011) 1272–1276.
- [30] H. Jónsson, G. Mills, K.W. Jacobsen, Nudged elastic band method for finding minimum energy paths of transitions, in: Classical and Quantum Dynamics in Condensed Phase Simulations, WORLD SCIENTIFIC, 1998, pp. 385–404.
- [31] G. Lehmann, M. Taut, On the numerical calculation of the density of states and related properties, Phys. Status Solidi b 54 (2) (1972) 469–477.
- [32] W. Tang, E. Sanville, G. Henkelman, A grid-based bader analysis algorithm without lattice bias, J. Phys.: Condens. Matter 21 (8) (2009) 084204.
- [33] G.A. Elia, K. Marquardt, K. Hoeppner, S. Fantini, R. Lin, E. Knipping, W. Peters, J.F. Drillet, S. Passerini, R. Hahn, An overview and future perspectives of aluminum batteries, Adv. Mater. 28 (35) (2016) 7564–7579.

- [34] L. Geng, G. Lv, X. Xing, J. Guo, Reversible electrochemical intercalation of aluminum in Mo6S8, Chem. Mater. 27 (14) (2015) 4926–4929.
- [35] V. Chevrier, S. Ong, R. Armiento, M. Chan, G. Ceder, Hybrid density functional calculations of redox potentials and formation energies of transition metal compounds, Phys. Rev. B: Condens. Matter Mater. Phys. 82 (7) (2010) 1–11.
- [36] A. Chakraborty, M. Dixit, D. Aurbach, D.T. Major, Predicting accurate cathode properties of layered oxide materials using the SCAN meta-GGA density functional, Npj. Comput. Mater. 4 (1) (2018) 46–49.
- [37] R. Shepard, M. Smeu, Ab initio investigation of α- and ζ-V2O5 for beyond lithium ion battery cathodes, J. Power Sources 472 (2020).
- [38] T.R. Juran, M. Smeu, Hybrid density functional theory modeling of Ca, Zn, and Al ion batteries using the Chevrel phase Mo6S8 cathode, Phys. Chem. Chem. Phys. 19 (31) (2017) 20684–20690.
- [39] S. Grimme, J. Antony, S. Ehrlich, H. Krieg, A consistent and accurate ab initio parametrization of density functional dispersion correction (DFT-D) for the 94 elements H-Pu, J. Chem. Phys. 132 (15) (2010).
- [40] S. Dudarev, G. Botton, Electron-energy-loss spectra and the structural stability of nickel oxide: An LSDA+U study, Phys. Rev. B: Condens. Matter Mater. Phys. 57 (3) (1998) 1505–1509.

- [41] J. Sun, A. Ruzsinszky, J. Perdew, Strongly constrained and appropriately normed semilocal density functional, Phys. Rev. Lett. 115 (3) (2015) 1–6.
- [42] V. Imandi, M.S.P. Jagannath, A. Chatterjee, Role of solvent in metal-on-metal surface diffusion: A case for rational solvent selection for materials synthesis, Surf. Sci. 675 (April) (2018) 54–63.
- [43] S.D. Perera, R.B. Archer, C.A. Damin, R. Mendoza-Cruz, C.P. Rhodes, Controlling interlayer interactions in vanadium pentoxide-poly(ethylene oxide) nanocomposites for enhanced magnesium-ion charge transport and storage, J. Power Sources 343 (2017) 580–591.
- [44] C. Bommier, X. Ji, Recent development on anodes for Na-ion batteries, Isrl. J. Chem. 55 (5) (2015) 486–507.
- [45] N. Singh, C.T. Campbell, A simple bond-additivity model explains large decreases in heats of adsorption in solvents versus gas phase: A case study with phenol on Pt(111) in water, ACS Catal. (2019) 8116–8127.
- [46] T.R. Juran, M. Smeu, TiSe2 cathode for beyond li-ion batteries, J. Power Sources 436 (2019) 226813.